The Measurement of the Heat-Transfer Coefficient between High-Temperature Liquids and Solid Surfaces

T.A. UTIGARD, A. WARCZOK, and P. DESCLAUX

Two experimental techniques were developed for the purpose of measuring the heat-transfer coefficient between liquid slags/salts and solid surfaces. This was carried out because the heat-transfer coefficient is important for the design and operation of metallurgical reactors. A "cold-finger" technique was developed for the purpose of carrying out heat-transfer measurements during steady-state conditions simulating heat fluxes through furnace sidewalls. A lump capacitance method was developed and tested for the purpose of simulating transient conditions. To determine the effect of fluid flow on the heat-transfer coefficient, nitrogen gas stirring was used. The two techniques were tested in molten (1) and $NaNO_3$, (2) NaCl, (3) Na_3AlF_6, and (4) $2FeO \cdot SiO_2$, giving consistent results. It was found that the heat-transfer coefficient increases with increasing bath superheat and stirring.

I. INTRODUCTION

FOR the design and operation of metallurgical processes, such as reverberatory and electric arc furnaces for calcine smelting, slag cleaning and flash furnaces, and electrolytic aluminum cells, several heat-transfer considerations are of great importance. In these reactors, long service life can only be achieved by the formation of a solid layer of slag/bath on the furnace sidewall, protecting the refractory from the very corrosive liquids. As illustrated in Figure 1, the sidewall heat flux in industrial furnaces varies greatly from 1 to 300 kW/m^2.[1] In the case of low heat fluxes, the sidewall may consist simply of insulating and refractory bricks, while for the very high intensity processes, intensively water-cooled copper panels are required.

In the Hall-Heroult process for the electrolytic production of aluminum in a molten cryolite-base electrolyte at about 960 °C, a side freeze forms along the sidewall of the furnace at a heat flux of 1.5 to 5 kW/m^2. Because this freeze protects the furnace lining, several investigators[2–15] have studied the heat-transfer phenomena taking place in the cell. The investigation by Taylor and Welch[8,11] appears to have produced fairly reliable data during steady-state measurements. An internally argon-cooled graphite cylinder was immersed into a cryolite melt until steady-state heat-transfer conditions were achieved. The cylinder was pulled out of the melt and allowed to cool, followed by the measurement of the ledge thickness which was typically 1.0 to 1.5 mm. Because they did not measure the total heat flux, they depended on the measurement of the ledge thickness as well as assuming a value of the thermal conductivity of the ledge, to calculate the heat-transfer coefficient. Using a ledge thermal conductivity of 0.759 W/m K, they calculated the heat-transfer coefficient to be approximately 608 W/m^2 K. They also reported that the heat-transfer coefficient increased from 34 to 45 pct with a fluid flow of 0.09 to 0.12 m/s.

Based on measurements in industrial cells which were carried out just above the bath/metal interface, the heat-transfer coefficient was calculated to be in the range from 550 to 1820 W/m^2 K with an average value of 1200 W/m^2 K.[8] The data indicate that the heat-transfer coefficient measured between liquid cryolite and the carbon sidewall is in the same range as that measured between liquid and solid bath. The data are fairly scattered owing to the dynamics of ledge growth and remelting causing difficulties in positioning of the thermocouple tip. The experiments by Gan and Thonstad[13] and by Taylor *et al.*[11] appear to be sound and representative for rapid freeze formation and remelting upon immersion of a cold specimen into the liquid bath. In calculating the heat-transfer coefficient using this technique, it was assumed that the heat effects associated with the freezing and remelting processes cancel out. As demonstrated later, this may not be a valid assumption.

Bagha *et al.*[16] estimated the heat-transfer coefficient between CaO-SiO_2-Na_2O slags and a copper cylinder to be in the range from 1800 to 3500 W/m^2 K based on a series of experiments simulating continuous casting. Scholey *et al.*[17] investigated the heat transfer in water-cooled zinc-fuming jackets and estimated the heat-transfer coefficient between liquid and solid slag to be 1100 W/m^2 K. The corresponding heat flux was in the range from 80 to 130 kW/m^2. Mikrovas *et al.*[18] measured the effective thermal conductivity of liquid slags by immersing copper cylinders into liquid slags (SiO_2-CaO-Al_2O_3-TiO_2). Based on their results, the heat-transfer coefficient is estimated to be in the range from 2000 to 3000 kW/m^2 K during the initial heat up to approximately 1100 °C. Nauman *et al.*[19] measured the rate of heating nickel spheres immersed into various ferrous silicates. By assuming that the interface temperature and the heat-transfer coefficient remain constant during the heat-up process, the average heat-transfer coefficient was calculated based on the time required to heat up the nickel sphere to the liquidus temperature.

Figure 2 shows a plot of the heat-transfer coefficients of the cryolite and ferrous silicate systems *vs* the overall

T.A. UTIGARD, Assistant Professor, and A. WARCZOK, Research Associate, are with the Department of Metallurgy, University of Toronto, Toronto, ON M5S 1H4, Canada. P. DESCLAUX, Consultant, is with Arvida Research and Development Centre, Alcan International Ltd., Jonquiere, PQ G7S 4K8, Canada.

Manuscript submitted September 11, 1992.

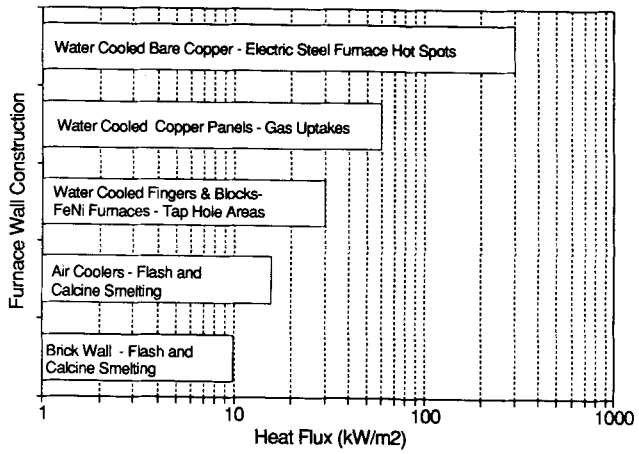

Fig. 1—Typical heat flux data for a wide range of industrial processes. The type of technology used to contain the various fluids is also indicated.[1]

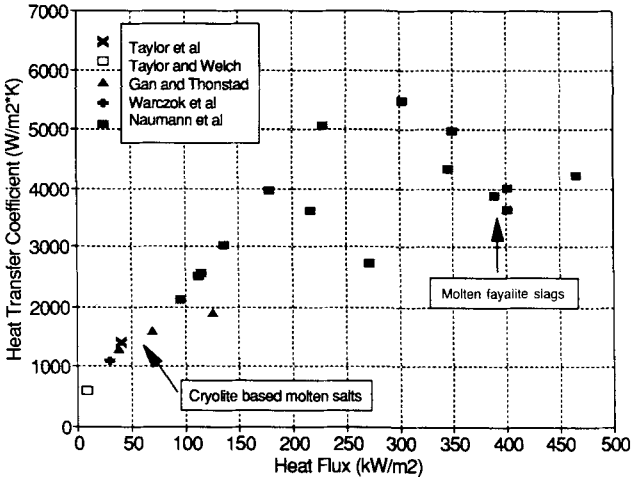

Fig. 2—Heat-transfer coefficient as a function of the average heat flux for molten cryolite[8,12,13,15] and fayalite.[19] The data for heat fluxes above 20 kW/m^2 originate from experiments where cold specimens were immersed into liquid cryolite[12,13] and fayalite.

heat flux. These values were calculated based on the reviewed literature data.[8,12,13,15,19] The heat-transfer coefficient increases with the overall heat flux for both systems, and the data for the slags seem to extend the values for cryolite to higher heat fluxes and heat-transfer coefficients. For fayalite-type slags, the heat-transfer coefficient increases from approximately 2000 to 5000 W/m^2 K with increasing heat flux from 100 to 400 kW/m^2, while for cryolite, it increases from approximately 600 to 1900 W/m^2 K with increasing heat flux from 10 to 130 kW/m^2. Based on this review, the following is concluded.

(1) The heat-transfer coefficient increases with increasing heat flux.
(2) Most laboratory experiments have been carried out under nonsteady conditions and at heat fluxes up to 400 kW/m^2; while in industrial aluminum cells and copper/nickel smelting furnaces, the heat flux is generally less than 10 kW/m^2.
(3) There is no significant difference between the heat-transfer coefficients measured with and without a ledge.
(4) Very few experimental investigations have been carried out.

When a liquid is flowing past a plate of a different temperature, a heat exchange takes place. The heat flux from the plate is given by the following equation:

$$q/A = h(T_{wall} - T_{liquid}) \quad [1]$$

where h is the heat-transfer coefficient. A series of expressions based on dimensionless numbers exist for the estimation of the heat-transfer coefficient as a function of the fluid conditions. Because of the undefined behavior of the fluid flow in most metallurgical reactors [flow is caused by (1) magnetic forces, (2) gas evolution or gas injection, (3) temperature and composition gradients, (4) interfacial tension gradients, and (5) solids feeding or slag pour backs], it is very difficult, if not impossible, to calculate the heat-transfer coefficient. Another limitation of these expressions is that they do not deal with transient phenomena, such as freezing or melting of the slag. To address these issues, this investigation was initiated. The main aim of this study was to develop a technique which would enable us to measure the heat-transfer coefficient between various liquids and solid surfaces at elevated temperatures both under laboratory and industrial conditions.

II. EXPERIMENTAL

Two techniques have been developed and tested: (1) a ('cold-finger') technique for the continuous measurement of the heat-transfer coefficient at heat fluxes more representative to plant conditions and (2) a nonsteady-state lump capacitance technique for measurements during the heating up of a cold specimen. In this manner, the results from two very different techniques could be compared and analyzed.

Heat-transfer coefficients are strongly dependent on the fluid flow. However, it is very difficult to determine the fluid velocity and the turbulence in an industrial furnace. The undefined nature and multitude of driving forces are typical for most metallurgical reactors and not the exception. To address this, the experiments were carried under "controlled" gas stirring conditions by bubbling argon through the melt at a given depth. The stirring energy is often the only information available, and it is used to (a) estimate mixing times in reactors[20] and (b) design electric furnaces for calcine smelting (maximum kilowatts per unit area of the furnace). The energy dissipation in the melt due to gas injection is given by.[20]

$$\text{Power } (W) = 738QT \times \ln(1 + 9.67 \times 10^{-4} \rho L) \quad [2]$$

where Q is the gas flow rate (Nm^3/s), T is the temperature in kelvin, ρ is the density (g/cm^3), and L is the lance immersion in centimeters. The energy dissipation due to the anode gas release in a Hall-Heroult cell is approximately 15 to 30 W/ton of liquid electrolyte and aluminum. For steelmaking processes with gas injection, the corresponding energy varies generally from 500 to more than 10,000 W/ton.[20]

A. *Cold-Finger Technique*

In order to develop a steady-state technique, a cold-finger method was built. The following molten salt/slag systems were tested.

Liquid Mixture	Temperature Range (°C)	Crucible Material
$NaNO_3$	305 to 400	graphite
NaCl	800 to 950	graphite
Na_3AlF_6	970 to 1060	graphite
Fe_2SiO_4	1180 to 1260	iron

The experimental setup is shown in Figure 3. The data were continuously recorded using an A/D converter DASCON-1 card and a multiplexer/amplifier EXP-16 card. The frequency of data sampling was 3 Hz. The cold finger is made from a 13-cm-high graphite crucible with inner and outer diameters of 1.98 and 2.56 cm, respectively. A thermocouple is located at the interface between the crucible wall and the inner thermal insulation as well as inside the graphite finger wall. A copper-tube cooling system is located in the center of the cold finger and is thermally insulated from the graphite finger by means of an insulating brick. Water flows down into the cold finger inside one copper tube (0.6-cm OD) and out through another. The heat flux is calculated based on the water flow rate and the difference in the water temperature between the inlet and outlet. Two RTD sensors are placed inside the copper tubes at the height of the cryolite bath to measure the water temperatures (±0.2 °C) at the inlet and outlet of the finger. Calibration experiments with thermal insulation around the finger were carried out in air at 1000 °C in order to evaluate the ('background') heat flow. This heat flow (≈8 W) was then subtracted from the heat flow measured (80 to 200 W) upon immersion into cryolite and NaCl baths at 800 °C to 1060 °C.

The graphite crucible (10-cm diameter and 14-cm height) containing approximately 1.8 kg of bath is located in an INCONEL* container and heated in a vertical pot furnace. Nitrogen gas was used to protect the graphite crucibles. The stainless steel support for the cold finger is designed to lock into the top of the graphite crucible. Thermal insulation between the top of the cold finger and the stainless steel support minimizes the heat loss from the melt. A series of K-type thermocouples are positioned at determined distances from the graphite cold finger at a depth of approximately 5 cm below the bath level. These thermocouples are protected using a 0.1-cm OD INCONEL sheet placed inside alumina tubes.

*INCONEL is a trademark of Inco Alloys International, Inc., Huntington, WV.

1. *Procedure*

The salt systems were prepared by mixing reagent grade chemicals in the required amounts. The synthetic fayalite slags were prepared by mixing iron powder, Fe_2O_3, and SiO_2 in stoichiometric proportions to form $2FeO \times SiO_2$ and melted in a graphite-clay crucible at 1325 °C in an argon atmosphere. The final synthetic fayalite was found to contain 1.5 pct Fe_3O_4 and 29.5 pct SiO_2. After keeping the melt at this temperature for approximately 20 minutes, the stainless steel support and the cold finger were lowered into the furnace until the graphite cold finger reached the set immersion depth (11 to 12 cm). The water flow and the thermocouple readings are continuously measured and stored using the data acquisition system. Typically, the experiments are carried out at one fixed bath temperature until steady state is achieved (≈5 to 10 minutes). In other experiments, gas stirring was introduced, and the resulting changes in the temperatures and the heat flux were monitored. The cold finger was occasionally pulled out of the melt to confirm that there was no frozen salt along the sides of the graphite finger.

2. *Calculation procedure*

At steady state, the heat flux is given by the following equation:

$$q = \frac{2 \times \pi \times H \times (T_{bath} - T_{water})}{\frac{1}{h_W \times r_{Cu}} + \frac{\ln\left(\frac{r_{ins}}{r_{Cu}}\right)}{k_{ins}} + \frac{\ln\left(\frac{r_C}{r_{ins}}\right)}{k_C} + \frac{1}{h_B \times r_L}} \quad [3]$$

where q is the heat output (W), T_B is the bath temperature (°C), T_w is the cooling water temperature (°C), H is the immersion depth (m), h_W is the water-copper heat-transfer coefficient (W/m^2 K), r_{Cu} is the copper tube radius (m), k_{ins} is the insulation thermal conductivity (W/m^2 K), r_{ins} is the radius of insulating brick (r), r_C is the graphite cylinder radius (m), and h_B is the bath/ledge heat-transfer coefficient (W/m^2 K). The first three terms in the denominator represent the cold-finger thermal resistance which is independent of any ledge or the fluid flow in the crucible. In this investigation, only data from tests where no freeze was formed will be presented and analyzed. The reasons for this are as follows:

(1) it is not required to assume a temperature for the bath/ledge interface;
(2) it is not required to measure the ledge thickness and to accurately know/measure the ledge thermal conductivity;
(3) the industrial data by Taylor[8] indicate that there is no significant difference between the heat-transfer coefficients measured with and without a ledge; and
(4) to compare the values with those measured with the lump technique.

By the measurement of the total heat flux and the carbon wall and bath temperatures, the heat-transfer coefficient between the bath and the graphite finger is calculated as follows:

$$h = \frac{q}{r_C} \times \left[2\pi \times H \times (T_B - T_1) - \frac{q}{k_C} \times \ln\left(\frac{r_C}{r_1}\right) \right] \quad [4]$$

where T_1 is the graphite temperature (°C) at the location of the thermocouple and r_1 is the location of the thermocouple in the graphite wall (m).

3. *Experimental testing*

The experimentally determined temperatures upon immersion of the cold finger into liquid NaCl are shown in

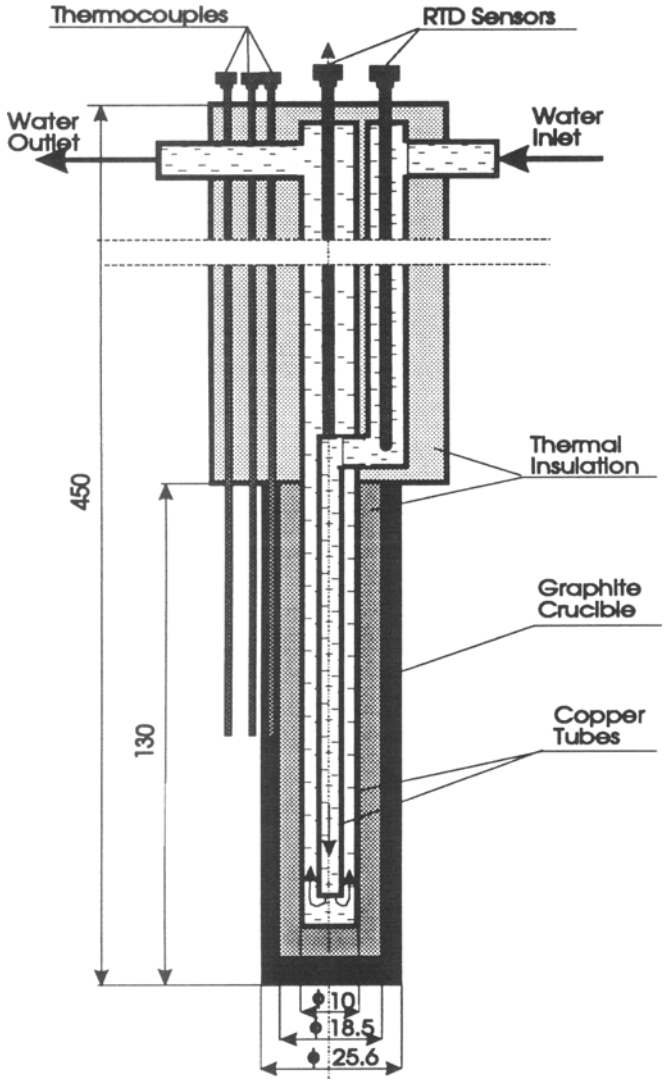

Fig. 3—Description of the cold-finger technique. A data acquisition system was used to record all experimental data. The graphite cold finger is placed in a 10-cm-diameter crucible which is placed in a top-loading laboratory furnace.

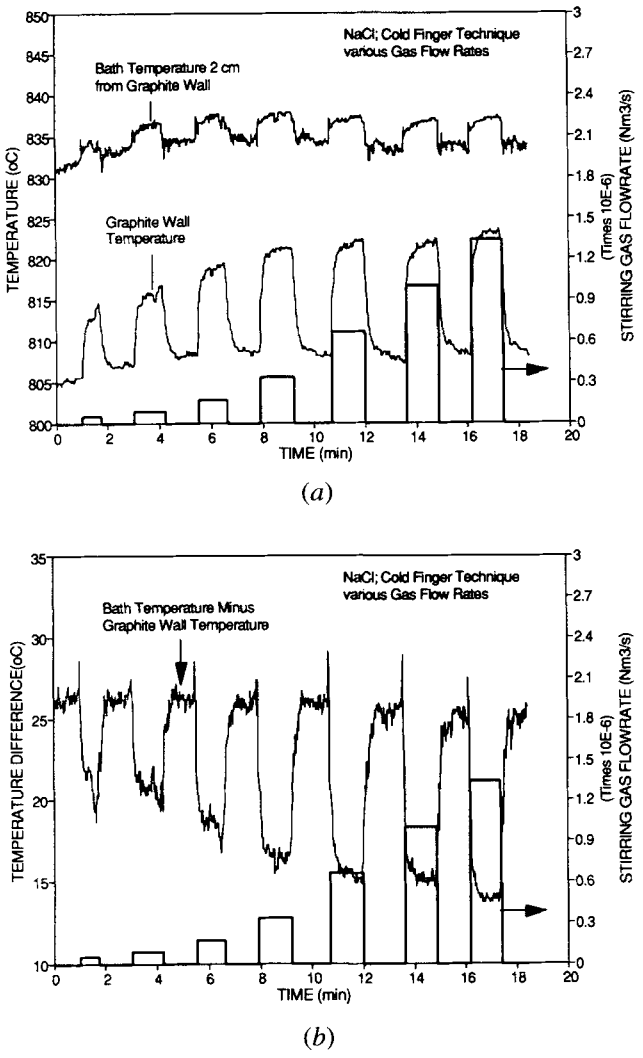

Fig. 4—(*a*) Bath and graphite finger temperatures upon immersion into NaCl at various degrees of stirring. (*b*) Bath temperature minus the graphite wall temperature as a function of time and stirring.

Figures 4(a) and (b). The average heat output during this particular experiment was 77.1 W with a standard deviation of 6.3 W. Based on Figures 4(a) and (b), the following observations are made.

(1) The bath and wall temperatures react almost instantaneously to the gas stirring.
(2) The difference between the bath and wall temperatures reaches steady state after approximately 1 minute upon changes to the stirring conditions.
(3) Increased stirring leads to a decrease in the temperature difference between the bath and the graphite wall.

It must be noted that the bulk of the thermal resistance of the cold finger is due to its insulation. Therefore, the overall heat flux remains almost constant for a given bath temperature. Increased bath stirring will not affect the absolute heat flux. As the heat-transfer coefficient increases with increasing stirring, the difference in the temperature will decrease correspondingly. The slight increase (2 °C to 3 °C) in the bulk bath temperature with gas stirring is thought to be due to slight temperature gradients in the bath before gas stirring.

The experimentally determined temperatures upon immersion of the cold finger in liquid cryolite with no gas stirring are shown in Figures 5(a) and (b). In this case, there is no frozen ledge at steady state after approximately 4 minutes. Figure 5(a) shows the rapid temperature response upon immersion of the cold finger into the liquid cryolite. The thermocouple farthest away from the graphite wall reaches the bath temperature almost immediately. After approximately 2 minutes, the thermocouples in the vicinity of the finger wall also reach the bath temperature. The wall temperature reaches steady state after approximately 4 minutes and remains below the bath temperature due to the internal cooling. Upon removal of the finger, the temperatures drop rapidly.

Figure 5(b) shows a detailed view of the changes in the temperature with time. From approximately 1 to 2.5 minutes after immersion, the overall bath temperature decreases due to the heat load required to heat the cold finger to steady state. This is followed by a slow

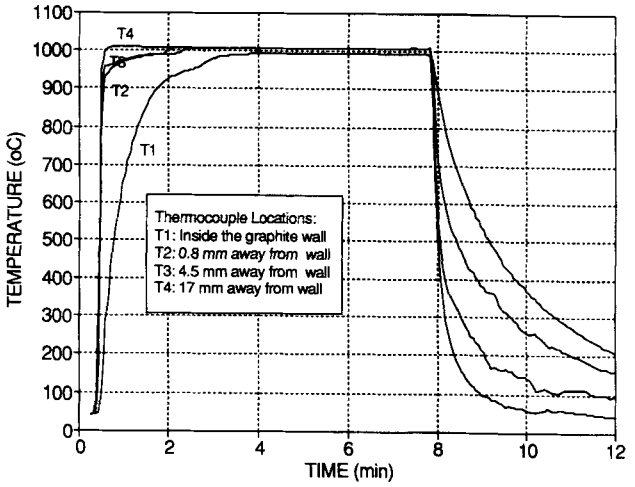

(*a*)

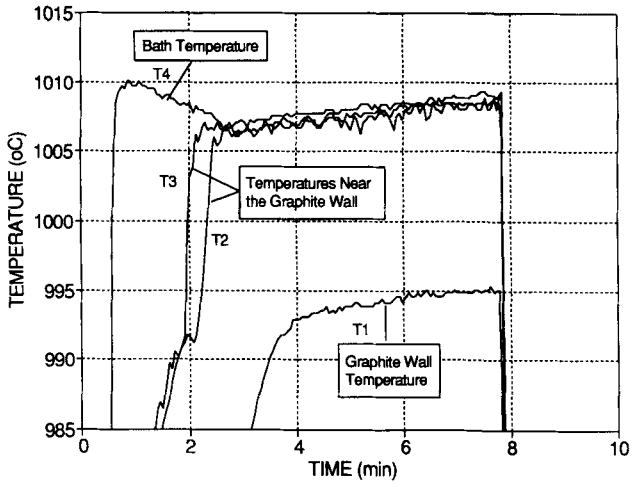

(*b*)

Fig. 5—(*a*) Bath and graphite wall temperatures upon immersion of the cold finger into liquid cryolite (Na_3AlF_6). (*b*) A detailed view of the bath and graphite wall temperatures upon immersion into liquid cryolite.

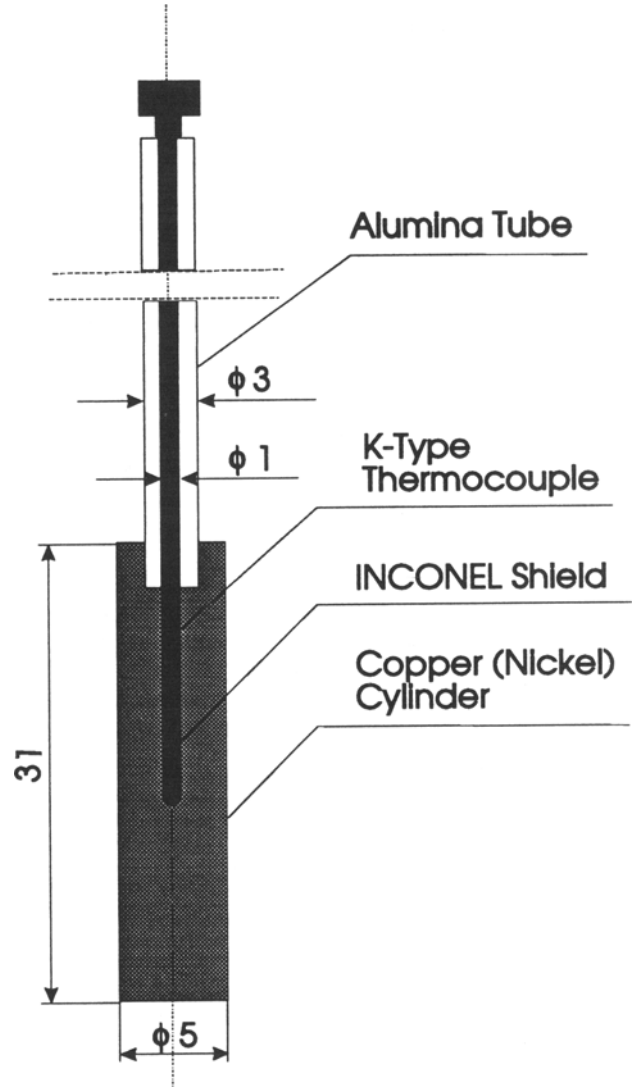

Fig. 6—Details of sensors used for the lump capacitance technique.

increase of all the temperature readings. The very small difference between the three thermocouples located in the bath indicates a uniform bath temperature. Based on the difference between the wall and bath temperatures, the heat-transfer coefficient is calculated using Eq. [4].

B. *Lump Capacitance Technique*

The main purposes of developing this technique were (1) to get a comparison with the cold-finger technique and (2) to potentially adapt it to plant experimentation because it is simple and safe and does not involve the use of water. It also simulates the heat-up process of solid-feed materials added to a furnace. Details of the copper and nickel sensors used are shown in Figure 6.

1. *Procedure*

After keeping the salt/slag at its temperature for approximately 20 minutes, the sensor was immersed at a speed of approximately 10 cm/s into the liquid by a computer-controlled arm. The immersion and duration (~2 minutes) of the experiment were controlled from a computer. In some experiments, the sensor was removed before complete remelting of the freeze for the purpose of investigating the freeze formation and remelting characteristics as well as the smoothness of the freeze surface. The salt/slag temperature, sensor temperature, and temperature in the vicinity of the cylinder were continuously recorded and stored during the experiments. The temperature of the sensor is measured by a-K-type thermocouple which is located in the center of the cylindrical sensor. The thermocouple was protected by a 1.0-mm-OD INCONEL sheet which was placed inside an alumina capillary. Two additional S-type thermocouples are used to control/measure the furnace and liquid temperatures. Nitrogen gas was used as an inert atmosphere, and in some experiments, it was used to stir the melt.

2. *Experimental testing*

Based on a large number of experiments in various slags and molten salts, it was shown that the heating up of the sensor takes place as follows.

(1) There is an instantaneous freeze formation of solid salt/slag.
(2) The freeze thickness grows, and the sensor heats up rapidly.
(3) At a given point, the freeze reaches a maximum thickness before it starts to melt back as the sensor gets hotter.
(4) Visual observations in NaCl, $NaNO_3$, and water/ice show that during the final remelting process, the upper part of the sensor becomes bare, and the remaining solid/mushy freeze suddenly slips away from the sensor.
(5) During the final heating up of the sensor after reaching the liquidus temperature, there is no remaining freeze.
(6) The sensor reaches the slag temperature.

This is illustrated in Figure 7 together with the measured temperature rise of a nickel cylinder immersed into fayalite with time. This behavior was confirmed experimentally by removing the nickel sensor at various times after immersion. Further confirmations were made by video recordings of the freezing/remelting process in molten NaCl and $NaNO_3$ melts at 850 °C and 350 °C, respectively. The initial rapid heating up is mainly due to the heat release from the slag upon solidification and cooling. The maximum freeze thickness is reached at approximately 20 seconds.

The Biot number for the copper-cylinder/molten mixture is given by

$$\mathrm{Bi} = \frac{h \times R}{k} \simeq \frac{1000 \times 2.5 \times 10^{-3}}{200} = 0.013 < 0.1$$

where h is the slag-freeze heat-transfer coefficient ($\approx$1000 W/m^2 K), R is the radius of the copper cylinder (2.5 mm), and k is the average thermal conductivity of copper from 25 °C to 1200 °C (200 W/m K). This shows that the sensor approximately has a uniform temperature at all times during heating. Therefore, the interface temperature between the sensor and the slag is assumed to be equal to that of the sensor measured by the thermocouple.

During the final heating up after the remelting of the frozen slag, the heat-transfer coefficient between the liquid and the solid sensor can be calculated as follows:

$$h \times \text{area} \times (T_{\text{slag}} - T_{\text{Ni}}) = C_p \times m_{\text{Ni}} \times \frac{dT_{\text{Ni}}}{dt} \quad [5]$$

where m_{Ni} is the mass of the nickel sensor. By integrating Eq. [5] the heat-transfer coefficient between the sensor and the liquid slag becomes

$$h = \frac{C_p \times m_{\text{Ni}}}{\text{area}} \times \frac{\ln [(T_{\text{slag}} - T_\circ)/(T_{\text{slag}} - T_{\text{Ni}}(t))]}{t} \quad [6]$$

where $C_{p,Ni}$ = 615 J/kg K at 1200 °C and $T_\circ$ is the nickel-cylinder temperature before immersion.

In order to study the effect of liquid flow on the heat-transfer coefficient, nitrogen gas was bubbled through the liquid. Based on several different sets of experiments, it was found that stirring did not affect the initial heat-up rate. This is consistent with the observations by Mikrovas *et al.*[18] It is only during the final remelting and heat-up stage that stirring leads to a faster heating up of the sample. Figure 8 shows the temperature of nickel cylinders immersed into fayalite with various gas injection rates. Also shown is the function $\{\ln [(T_{\text{slag}} - T_\circ)/(T_{\text{slag}} - T_{\text{Ni}}(t))]\}$ *vs* time. Subsequent to the remelting of the freeze at approximately 1170 °C to 1180 °C, the logarithm of this ratio becomes a linear function of the temperature. This shows that the heat-transfer coefficient remains constant within this temperature range, and from the slope of this line, the heat-transfer coefficient can be calculated. The data in Figure 8 show that the heat-transfer coefficient increases from 925 to 3290 W/m^2 K by injecting nitrogen at a flow rate of only 6.7×10^{-7} Nm^3/s. This increase is thought to be partly due to sensor vibrations induced by the gas bubbling.

Figure 9 shows the temperature of copper cylinders immersed in molten $NaNO_3$ at various gas injection rates. The function $\{\ln [(T_b - T_\circ)/(T_b - T_{\text{Cu}}(t))]\}$ becomes a linear function *vs* time subsequent of the remelting process at approximately 305 °C to 310 °C. The

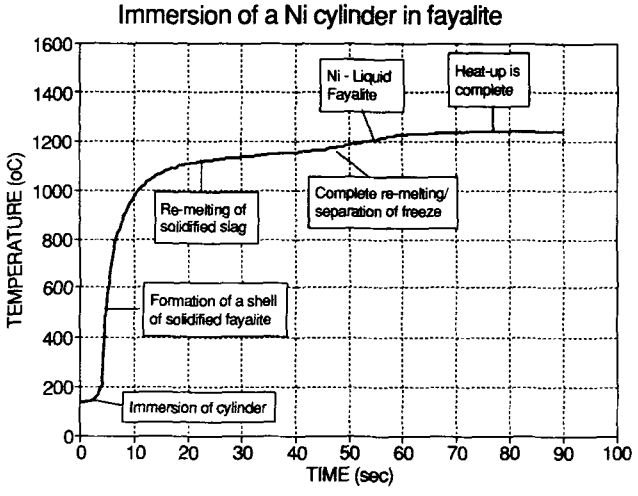

Fig. 7—Temperature rise of a nickel cylinder upon immersion into liquid fayalite at 1240 °C. The various physical phenomena taking place are superimposed on the experimental curve.

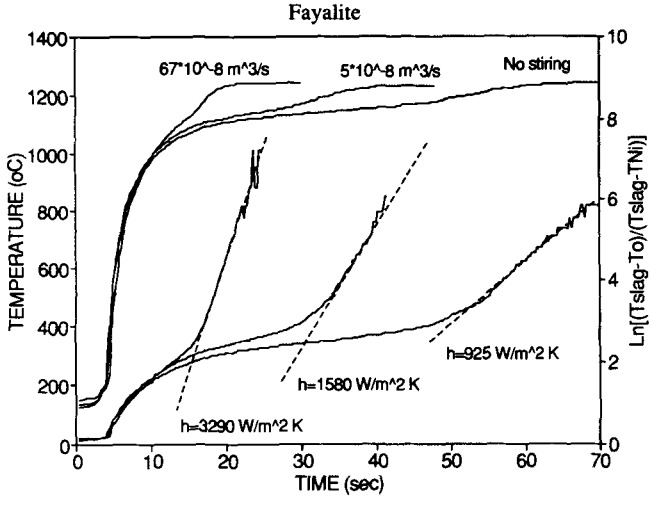

Fig. 8—Temperature rise of a nickel cylinder upon immersion into liquid fayalite with gas stirring. The calculated heat-transfer coefficients during the final heating-up stage are also indicated.

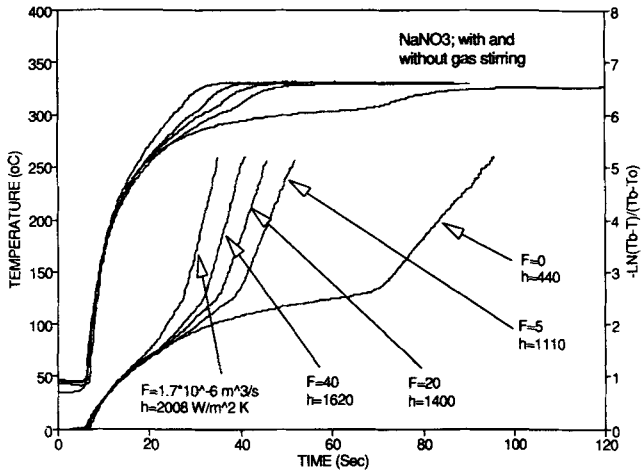

Fig. 9—Temperature rise of a copper cylinder upon immersion into liquid $NaNO_3$ with gas stirring. The calculated heat-transfer coefficients during the final heat-up stage are also indicated.

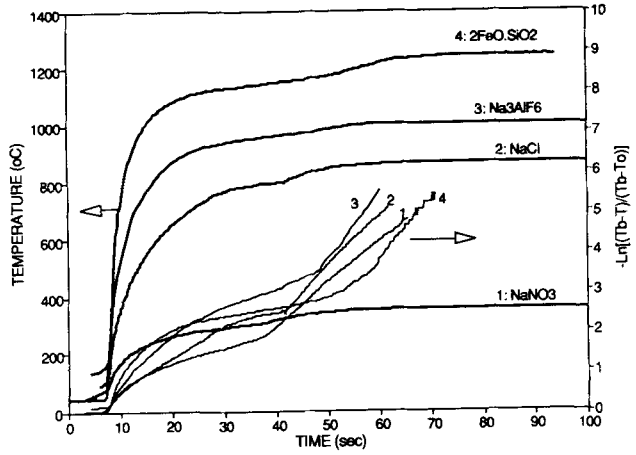

Fig. 10—Temperature rise of a copper cylinder upon immersion into (1) $NaNO_3$, (2) NaCl, and (3) Na_3AlF_6 at a superheat of 40 °C. Also included is the temperature rise of a nickel cylinder upon immersion into liquid fayalite (Fe_2SiO_4).

heat-transfer coefficient increases from 440 to 2008 W/m^2 K by injecting argon at a flow rate of only 1.67 $\times$ 10^{-6} Nm^3/s. Again, it is only during the final remelting and heat-up stage that stirring leads to a faster heating up of the sample.

Figure 10 shows that the heating up occurs in a similar fashion to the various melts tested. Because of temperature limitations, a nickel cylinder was used for the fayalite slag. These results indicate that the same phenomena take place in the various liquids and that the technique can be used over a wide range of temperatures and liquids.

III. DISCUSSION

The results obtained in $NaNO_3$ melts by using the two techniques are compared in Figure 11 as a function of the superheat. Using the cold-finger method, the superheat is defined as the temperature difference between the wall/bath interface and the bulk of the bath. For the lump capacitance technique, the superheat is defined as the bath temperature minus the liquidus temperature. Without stirring, the heat-transfer coefficient increases with increasing superheat. This is reasonable since the driving force for natural convection also increases with increasing temperature difference. A small amount of gas stirring greatly increases the heat-transfer coefficient as measured with the two techniques. For the cold-finger technique, the application of gas stirring leads to a drop in the superheat; *i.e.*, the graphite wall temperature increases. This is because the overall heat flux is nearly independent of the heat-transfer coefficient, and an increased heat-transfer coefficient leads to a drop in the superheat ($\Delta T \cdot h \sim$ constant).

Using the cold-finger technique, it is observed (Figure 12) that the heat-transfer coefficient between $NaNO_3$ and the graphite wall decreases with decreasing bath temperature under a constant bath superheat of 12 °C to 13 °C. This may be explained by the fact that the viscosity increases with decreasing temperature and

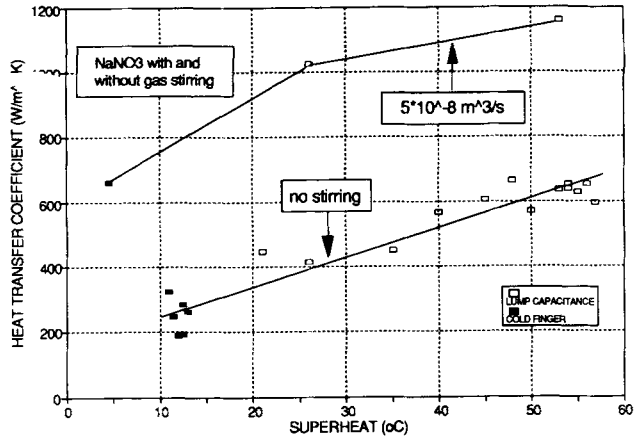

Fig. 11—A comparison of the heat-transfer coefficient in liquid $NaNO_3$ as measured by the two techniques with and without gas stirring.

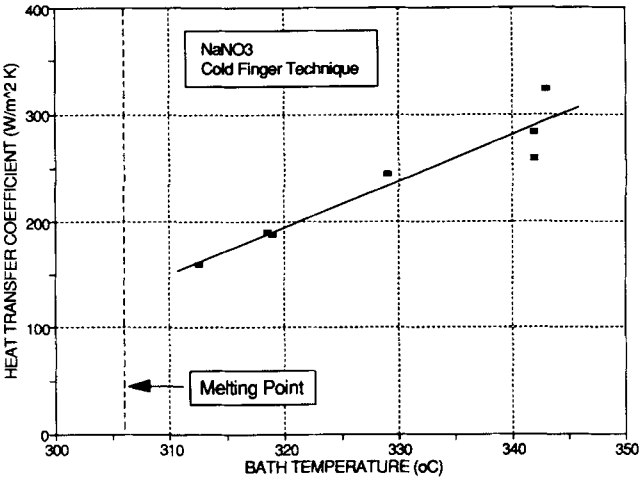

Fig. 12—Heat-transfer coefficient between graphite and liquid $NaNO_3$ as a function of the bath temperature.

possibly due to the formation of a "mushy" layer at the interface.

Figure 13 shows that the heat-transfer coefficient in liquid cryolite is strongly dependent on the bath stirring. Based on a regression analysis, the following equation was found:

$$h\ (\mathrm{W/m^2\ K}) = 919 + 25.6 \times \text{stirring energy}^{1/2} \quad [7]$$

where the stirring energy is given in W/tonne of liquid cryolite. Taylor[8,12] reported that the heat-transfer coefficient increased 34 to 45 pct for a fluid flow of 0.09 to 0.12 m/s. Because of the different methods used to induce fluid motion, it is not possible to compare the results directly. However, the increase in the heat-transfer coefficient is similar in both studies, and the range of values obtained in this investigation compares well with the data of Taylor.[8]

The heat-transfer coefficient measured during the final heating up of the nickel sensor in fayalite following the complete melting of the freeze is plotted in Figure 14 as a function of the heat flux and the slag superheat. For a fixed bath superheat, the heat flux (and the heat-transfer coefficient) was effectively increased by increasing bath stirring. Because at low superheats (10 K) the data are measured over a very small temperature range, quite a scatter was observed, and the accuracy is estimated to be only ±30 pct. The heat-transfer coefficient was found to increase with increased stirring and bath superheats.

In order to use a heat-transfer coefficient in an industrial furnace, knowledge of the bath and interface temperatures is required. For the cryolite-base systems, Haupin[21] noted that there appears to be quite an uncertainty regarding the measurement of the bath temperature and the calculated liquidus as based on the bath analysis. For the multicomponent slag/salt systems typical for industrial processes, only careful differential thermal analysis-type experiments can provide sufficient accurate temperature data. Because the location of the heat source is often away from the area of charge being smelted, which again may be away from the sidewall

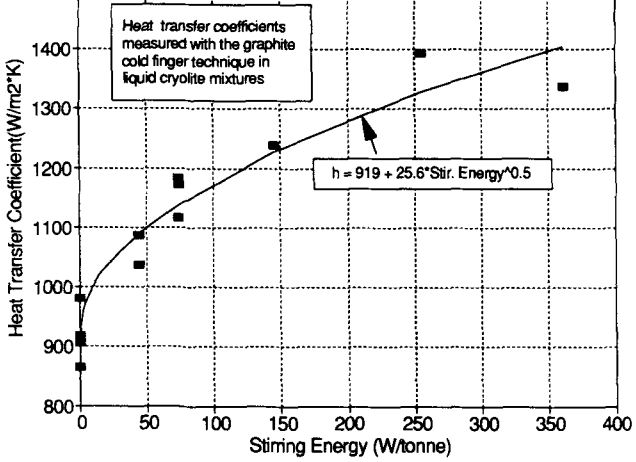

Fig. 13—Heat-transfer coefficient between graphite and liquid cryolite at 1008 °C as a function of the stirring energy. In this experiment, no ledge was present at steady state.

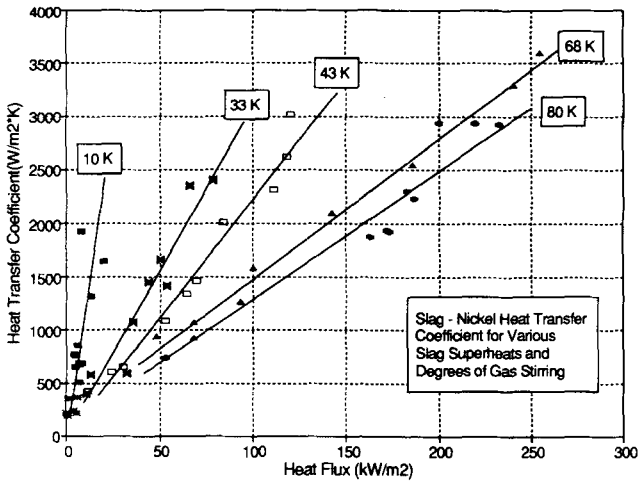

Fig. 14—Heat-transfer coefficient between liquid fayalite and nickel *vs* the absolute heat flux. For a fixed superheat, experiments were carried out with various degrees of melt stirring induced by gas injection.

areas, temperature gradients always exist, leading to significant variations in the viscosity. Together with the variations in the fluid flow, it becomes an almost impossible task to accurately predict the local heat-transfer conditions. However, with the present techniques, it should be possible to carry out plant measurements for a wide range of reactors.

IV. CONCLUSIONS

Two separate experimental techniques have been developed for the purpose of measuring the heat-transfer coefficient between liquid salts/slags and solid metals. Using these two techniques, the heat-transfer coefficient can be measured (1) at steady state and (2) during the final heating up of a specimen above its liquidus temperature. The two techniques have been tested in molten $NaNO_3$, NaCl, Na_3AlF_6, and $2FeO \cdot SiO_2$.

The measurements show that the heat-transfer coefficient is strongly dependent on the liquid superheat and stirring and that it increases with increasing heat flux.

ACKNOWLEDGMENTS

The financial support from Alcan International Limited, the Centre of Chemical Process Metallurgy, Toronto, and the National Science and Engineering Research Council, Ottawa, is greatly appreciated.

REFERENCES

1. B. Wasmund: Hatch Associates, Toronto, Canada, private communication, July 1992.
2. W. Haupin: in *Light Metals*, T.G. Hdgeworth, ed., 100th AIME Annual Meeting, 1971, pp. 184-94.
3. J.G. Peacey and G.W. Medlin: in *Light Metals*, W.S. Peterson, ed., 108th AIME Annual Meeting, New Orleans, Feb. 1979, pp. 475-92.
4. H. Tsukahara, N. Ono, and K. Fujita: in *Light Metals*, J.E. Andersen, ed., 111th AIME Annual Meeting, Dallas, Feb. 1982, pp. 471-82.

5. J. Thonstad and S. Rolseth: in *Light Metals*, E.M. Adkins, ed., 112th AIME Annual Meeting, Atlanta, March 1983, pp. 415-24.
6. A. Solheim and J. Thonstad: in *Light Metals*, E.M. Adkins, ed., 112th AIME Annual Meeting, Atlanta, March 1983, pp. 425-35.
7. M.P. Taylor, B.J. Welch, and J.T. Keniry: in *Light Metals*, E.M. Adkins, ed., 112th AIME Annual Meeting, Atlanta, March 1983, pp. 437-47.
8. M.P. Taylor: Ph.D. Thesis, The University of Auckland, Auckland, New Zealand, 1984.
9. T. Ohta and T. Matsushima: in *Light Metals*, J.P. McGeer, ed., 113th AIME Annual Meeting, Los Angeles, Feb. 1984, pp. 689-99.
10. W. Schmidt-Hatting, J.M. Blanc, J.C. Bessard, and R.V. Kaenel: in *Light Metals*, H.O. Bohner, ed., 114th AIME Annual Meeting, New York, Feb. 1985, pp. 609-24.
11. M.P. Taylor, B.J. Welch, and R. McKibbin: *AIChE J.*, 1986, vol. 32, pp. 1459-65.
12. M.P. Taylor and B.J. Welch: *Metall. Trans. B*, 1987, vol. 18B, pp. 391-98.
13. Y.R. Gan and J. Thonstad: in *Light Metals*, C.M. Bickert, ed., 119th AIME Annual Meeting, Anaheim, Feb. 1990, pp. 421-27.
14. T.A. Utigard, A. Warczok, and P. Desclaux: in *Extraction, Refining and Fabrication of Light Metals, Proceedings*, CIM Annual Meeting, Ottawa, Aug. 1991, vol. 24, pp. 163-76.
15. A. Warczok, T.A. Utigard, and P. Desclaux: in *Proceedings, The Savard/Lee Int. Symp. on Bath Smelting*, Montreal, Oct. 1992.
16. S. Bagha, N.C. Machingawuta, and P. Grieveson: in *Proceedings, 3rd Int. Conf. on Molten Slags and Fluxes*, June 1988, Glasgow, The Institute of Metals, M&A Thompson Litho Ltd., pp. 235-40.
17. K.E. Scholey, G.G. Richards, and I.V. Samarasekera: *Metall. Trans. B*, 1991, vol. 22B, pp. 163-75.
18. A.C. Mikrovas, S.A. Argyropoulos, and I.D. Sommerville: *Trans. ISS*, Dec. 1991, pp. 51-61.
19. J. Naumann, G. Foo, and J.F. Elliott: in *Extractive Metallurgy of Copper*, International Symposium, Las Vegas, 1976, The Metallurgical Soc. of AIME, J.C. Yannopoulos and J.C. Agarwal, eds., pp. 237-58.
20. N.J. Themelis and P. Goyal: *Can. Metall. Q.*, 1983, vol. 22, pp. 313-20.
21. W. Haupin: in *Light Metals*, E.R. Cutshall, ed., 121th AIME Annual Meeting, San Diego, March 1992, pp. 477-80.